Accelerating Motion Perception Model Mimics the Visual Neuronal Ensemble of Crab

Conference Paper · July 2022

DOI: 10.1109/IJCNN55064.2022.9892540

6 authors, including:

Hao Luan
Tianjin University of techonlogy and education
9 PUBLICATIONS **73** CITATIONS
SEE PROFILE

Mu Hua
University of Lincoln
12 PUBLICATIONS **29** CITATIONS
SEE PROFILE

Shigang Yue
University of Leicester
272 PUBLICATIONS **4,188** CITATIONS
SEE PROFILE

Accelerating Motion Perception Model Mimics the Visual Neuronal Ensemble of Crab

Hao Luan[1], Mu Hua[4], Jigen Peng[2,3], Shigang Yue[4], Shengyong Chen[1], Qinbing Fu[*,2,3,4]
[1]School of Computer Science and Engineering, Tianjin University of Technology, Tianjin, China
[2] School of Mathematics and Information Science, Guangzhou University, Guangzhou, China
[3] Machine Life and Intelligence Research Centre, Guangzhou University, Guangzhou, China
[4] School of Computer Science, University of Lincoln, Lincoln, UK

Abstract— In nature, crabs have a panoramic vision for the localization and perception of accelerating motion from local segments to global view in order to guide reactive behaviours including escape. The visual neuronal ensemble in crab plays crucial roles in such capability, however, has never been investigated and modelled as an artificial vision system. To bridge this gap, we propose an accelerating motion perception model (AMPM) mimicking the visual neuronal ensemble in crab. The AMPM includes two main parts, wherein the pre-synaptic network from the previous modelling work simulates 16 MLG1 neurons covering the entire view to localize moving objects. The emphasis herein is laid on the original modelling of MLG1s' post-synaptic network to perceive accelerating motions from a global view, which employs a novel spatial-temporal difference encoder (STDE), and an adaptive spiking threshold temporal difference encoder (AT-TDE). Specifically, the STDE transforms "time-to-travel" between activations of two successive segments of MLG1 into excitatory post-synaptic current (EPSC), which decays with the elapse of time. The AT-TDE in two directional, i.e., counter-clockwise and clockwise accelerating detectors guarantees "non-firing" to constant movements. Accordingly, the accelerating motion can be effectively localized and perceived by the whole network. The systematic experiments verified the feasibility and robustness of the proposed method. The model responses to translational accelerating motion also fit many of the explored physiological features of direction selective neurons in the lobula complex of crab (i.e. lobula complex direction cells, LCDCs). This modelling study not only provides a reasonable hypothesis for such biological neural pathways, but is also critical for developing a new neuromorphic sensor strategy.

Index Terms—neural modeling, visual neuronal ensemble, accelerating motion, spatial-temporal difference encoder, crab

I. Introduction

After millions of years of evolution, animals have developed powerful visual perception systems to guide their behaviours. Taking arthropods as a typical example, though compact as their brains are, they perform remarkably during foraging or predating, navigating and avoiding impending collision by exploiting their visual systems [1]–[5]. Within the complex visual pathways, multiple features of the collected motion cues are precisely extracted. Biologists have found various motion-sensitive neurons in arthropods' visual system, such as the lobula giant movement detectors (LGMDs, [6], [7]), the lobula plate tangential cells (LPTCs, [1], [9]), the small target motion detector (STMD, [10]), the monostratified lobula giant neurons(MLGs, [11]–[14]). Taking inspiration from above solid researches, a good number of excellent works on neural modeling have been proposed to explain how visual signals are processed [2], [3], [5], [15], and have been further optimized to be applied onto autonomous vehicles, demonstrating efficacy and effectiveness [8], [16]–[18], [22], [25].

Among aforementioned motion-sensitive neurons in arthropods, the sophisticated structure of monostratified lobula giant neurons type 1 (MLG1s) neuronal ensemble draws attention from both neuro- and computer scientists [12], [14], [15], [19]. Compared to the LGMD1 looming-sensitive neuron, which consists of one single neuron in lobula layer connected to post-synapses, the so-called MLG1s ensemble includes up to 16 MLG1 neurons covering the entire receptive field. As tangential neurons in lobules, MLG1s collect visual signals from columnar neurons associated with partial receptive fields. Thus, the MLG1s ensemble is thought to be a suitable candidate to localize a moving object [15]. Although the post-synaptic visual pathways of MLG1s ensemble remains unknown, it is suggested that visual signals are received by one special region located in the midbrain of a crab, together with nervous information, making difference to crabs' behaviours [15], [20].

Recent research has identified a group of remarkably directional selective (DS) neurons in crab Neohelice granulatus, named lobula complex directional cells (LCDCs, [21]) . Quite distinguished from DS neurons dedicated to processing of optical flow in most of arthropods, LCDCs in crabs take optical flow information in the meanwhile process object motion cues, with preference for horizontal movements [21]. As with MLG1s, the LCDCs also collect visual signals from the columnar neurons. Specifically, most of the LCDCs show similar features with motion-sensitive neurons (e.g. MLG1s): (a) each LCDC corresponding to partial receptive field. (b) strong responses to object moving. (c) rapid adaption to continuous stimuli. Whilst, the other LCDCs exhibit sustained responses to continuous stimuli (see Fig.1). Therefore, a reasonable hypothesis is that the accelerating motion could re-

activate the LCDCs which show adaptive responses to continuous stimuli. In other words, the LCDCs with sustained responses function as directional motion detectors whilst the LCDCs with adaptive responses are accelerating movement detectors. How to model such fascinating visual neuronal ensemble, however, leaves vacancy for bridging biological neural pathway to artificial vision system for solving real-world motion perception problems.

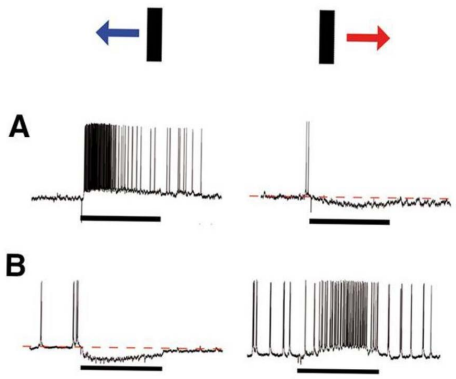

Fig. 1. Two LCDCs responses to horizontal object motions. Blue and red arrows indicate the directions of moving objects. LCDCs A and B have opposite motion directional preference. LCDC A shows a series spikes in burst at the beginning of the motion, whilst LCDC B shows a sustained response. Figure adapted from [21].

Inspired by the crab's visual pathways and MLG1 neurons, the previous computational MLG1s neural network realizes the localization of approaching object [19]. Within this study, we further develop the previous MLG1s model and propose an accelerating motion perception model (AMPM) to mimic the visual neuronal ensemble of crab. In contrast to the other bio-inspired motion-sensitive neuron models that only focus on the elementary motion patterns (e.g. size, direction, approaching and so on, [16]–[18], [22]–[24]), our proposed AMPM model aims to be one of the explorations of decoding a higher-level motion pattern, that is accelerating motion cues. In order to perceive the accelerating cues, the AMPM employs a novel spatial-temporal difference encoder (STDE), and an adaptive spiking threshold temporal difference encoder (AT-TDE). The former transforms "time-to-travel" between activations of successive segments of local MLG1 into excitatory post-synaptic current (EPSC), which decays with respect to time and generates spikes once reaching the threshold. The latter works effectively in two directional accelerating detectors to guarantee "non-firing" to constant movements from the global view. Accordingly, the AMPM can localize and perceive accelerating motion, which well reconciles with many of the revealed characteristics of neuronal ensemble in crab.

The details of the proposed method are elaborated as: Section II introduces the AMPM. In Section III, systematic experiments are carried out to validate the proposed method. Further discussions and conclusion are given in Section IV.

II. Framework of visual neuronal ensemble model

In this section, we briefly review the MLG1s neural network and introduce the AMPM which is based on STDE and AT-TDE in detail.

A. Pre-synaptic model: Encoding local motion

We previously proposed a MLG1s neural network, which is used for perceiving local approaching motions [19]. The MLG1s neural network modelled the crab's visual pathways in transferring optic signals from retina to lamina, medulla and lobula complex. Then, the single MLG1 neuron integrates the approaching motion cues and spike unit produces spikes to indicate looming event. The post-synaptic neural network, i.e. the looming spatial localization neural network (LSL), localized the spatial location of the approaching object. The AMPM model, as well as the LSL, is an another post-synaptic neural network of the MLG1s neuronal ensemble (see Fig.2(b)).

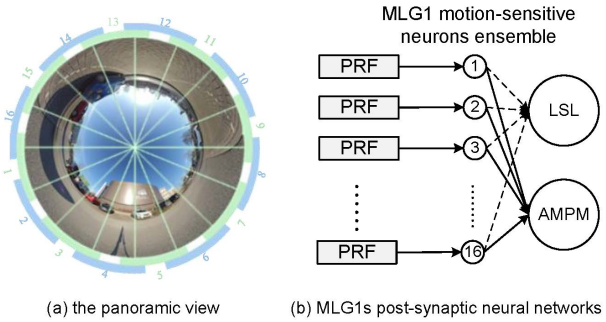

Fig. 2. Setting up the motion perception model: (a) the panoramic view has been evenly divided into 16 receptive fields. Each receptive field has overlaps with its two neighbours. (b) the relationship between the LSL neural network and AMPM model.

Because the crab has a monocular 360 deg receptive field, the panoramic view has been divided evenly into 16 segments in the MLG1s model, as shown in Fig.2(a). In the pre-synaptic neural network, each partial receptive field corresponding to one MLG1 neuron, where the motion patterns are sensed. The MLG1 in the model could be activated for: (a) an approaching event. (b) an object is coming into the MLG1 neuron's partial receptive field. The object coming-into event also has an expanding edges at the beginning of the motions. The systematic experiments verified the effectiveness of winner-take-all mechanism and looming-spatial-localization mechanism of the MLG1s neural network in localizing the local approaching object. But, these two mechanisms eliminate spatial-temporal motions cues. Therefore, we add a new mechanism before the spike unit, to adjust the model structure to make the previous model outputs suitable for our proposed AMPM. More specifically, the max3 mechanism is introduced to obtain three largest normalized membrane potential. Each

value in the vector V_{max3} could be defined by formula (1):

$$V_{max3}(i,t) = \begin{cases} 1, & \text{if } M(i,t) >= T_s \& \ M(i,t) > m_4(t) \\ 0, & \text{otherwise} \end{cases} \tag{1}$$

where i indicates the segment number of MLG1 neurons (i.e. $j = [1, 2, \cdots 16], i \in j$). $M(i,t)$ is the normalized membrane potential. $m_4(t)$ is the fourth largest value of the normalized membrane potential at the moment t. T_s provides the spiking threshold.

And then, the vector of spike unit V_{spike} can be defined as:

$$V_{spike}(i,t) = \begin{cases} 1, & if \sum_{i=t-N_t}^{t} V_{max3}(i,t) \geq n_{sp} \\ 0, & \text{otherwise} \end{cases} \tag{2}$$

where n_{sp} and N_t denote the number of successive spikes and frames, respectively. i indicates the segment number.

In the following of this paper, instead of the "MLG1s neural network", we will use the "pre-synaptic model" to refer to the adjusted MLG1s neural network.

B. Post-synaptic model: Perceiving global accelerating motion

Based on the pre-synaptic model, we design an AMPM for perceiving global accelerating motion. As the structure displayed in Fig.3, the pre-synaptic model's outputs (i.e. the vector output defined in equation (2)) will import into the post-synaptic model (i.e. the proposed AMPM).

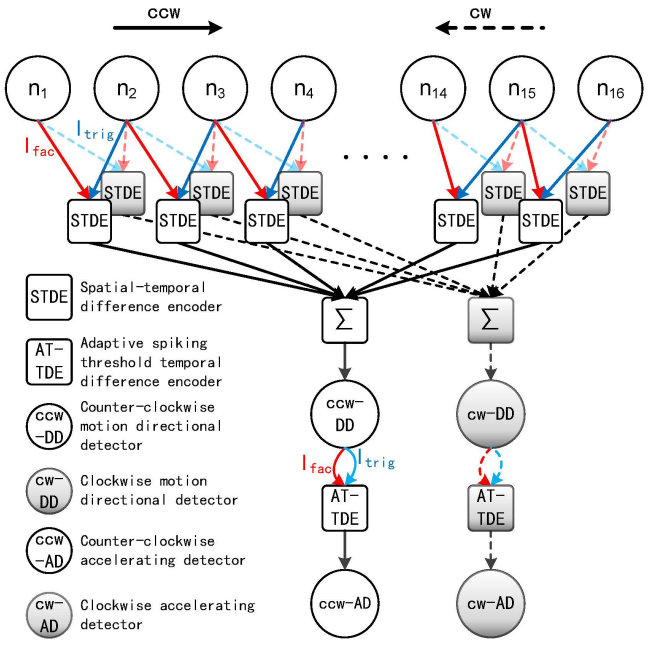

Fig. 3. Schematic diagram of the proposed AMPM. Each neuron $(n_1, n_2, \cdots)$ collects local motion information from the pre-synaptic model. For mimicking the crab's view, both clockwise and counter-clockwise accelerating translating motion can be decoded into spikes.

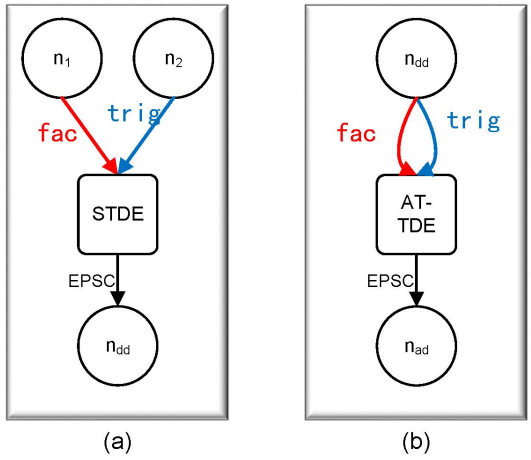

Fig. 4. Structures of STDE and AT-TDE units, respectively in (a) and (b). fac: facilitation. trig: trigger. EPSC: excitatory post synaptic current.

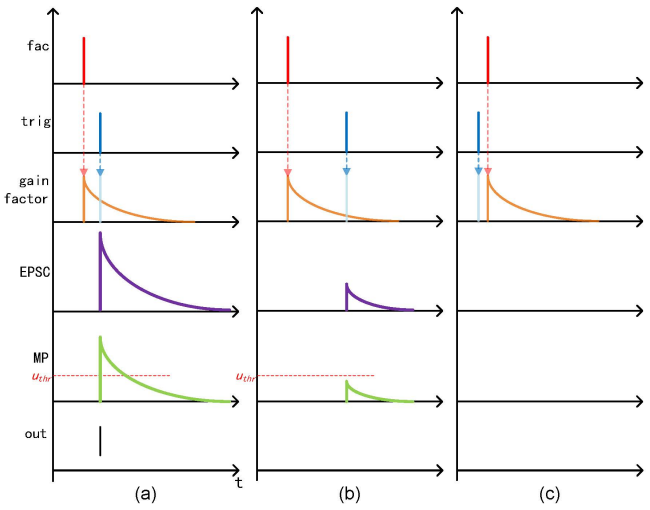

Fig. 5. The STDE transforms the time-to-travel between the two successive pulse (i.e. the facilitation and trigger pulses) into EPSC intensity. fac: facilitation. trig: trigger. EPSC: excitatory post synaptic current. MP: membrane potential. out: the neuronal spike output. A facilitation pulse initializes the gain factor, which decays over time. Whereafter, a trigger pulse is injected and amplified by the decaying gain factor. This leads to the EPSC, which fires the neuron to emit a spike. If the trigger pulse has a large temporal delay, or the trigger pulse is produced before the facilitation pulse, no neuronal spike will be generated (see (b) and (c)).

As illustrated in Fig.3, the translational motion direction has been set as clockwise (CW) and counter-clockwise (CCW), which are represented as dot and solid lines, respectively. Generally speaking, the model consists of: (a) the spatial-temporal difference encoders (STDE) to extract spatial and temporal motion cues between neighbouring neurons $(n_1, n_2, \cdots)$, then motion direction presents with spiking format in directional detectors (DD). (b) the adaptive spiking threshold temporal difference encoders (AT-TDE) encode the time-to-travel between two successive pulses, which produced by DD. The adap-

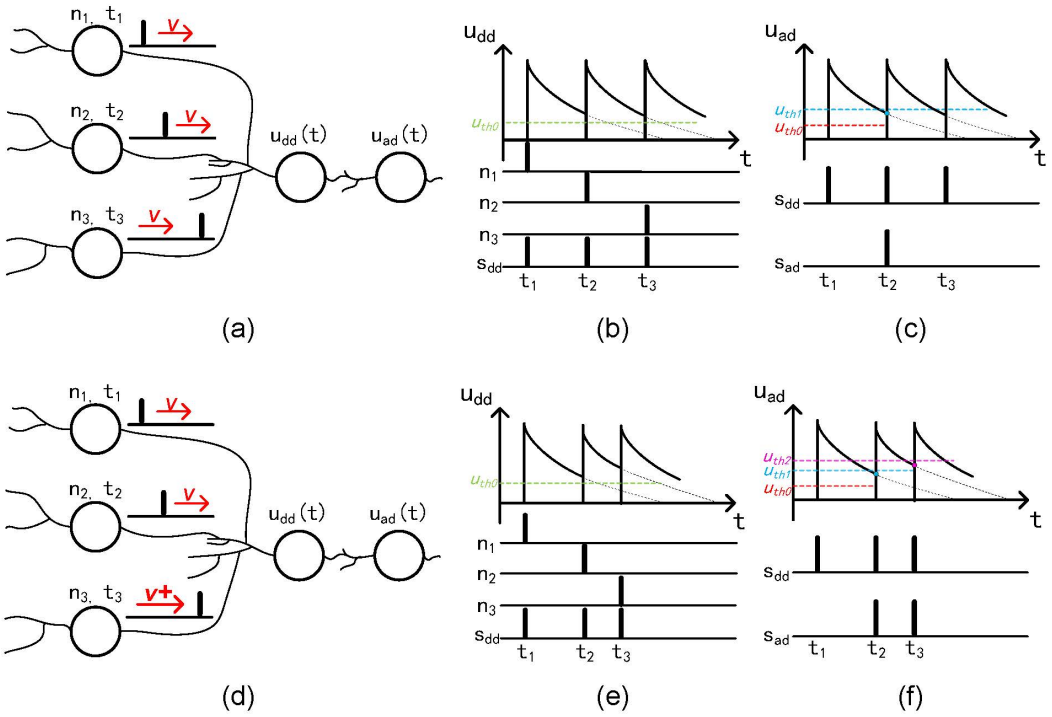

Fig. 6. Schematic diagram of neuronal pathways . The constant velocity and accelerating translational motions are presented respectively in (a) and (d). The STDE mechanism encodes two successive pulses which generated by the neighbouring neurons (see (b) and (e), s_{dd}). Only the accelerating translational motion could activates AT-TDE successively(see (f) s_{ad}). (b) The constant velocity translational motion elicits uniform pulses in time (see s_{dd} ax). (c) The uniform s_{dd} pulses elicit only one s_{ad} pulse when the u_{ad} firstly exceed the red threshold u_{th0}. And then, the threshold has been set as blue threshold u_{th1}. Thus, the constant velocity motion couldn't activate the accelerating detector again. (e) The accelerating translational motion produces faster pulses than constant motion (see s_{dd} axes respectively in (b) and (e)). (f) Similar to the neuronal response in constant motion, the accelerating detector has been activated when the u_{ad} exceeds the threshold. However, the faster pulse could activate the accelerating detector again. So, the accelerating detector produces more pulses while processing accelerating motion (see s_{ad}). u_{dd}: membrane potential of directional detector. u_{ad}: membrane potential of accelerating detector. s_{dd}: spike of directional detector. s_{ad}: spike of accelerating detector. X-axes: time.

tive spiking threshold mechanism (AT) is used to inhibit spikes elicited by constant and deceleration motions. The STDEs provide a horizontal direction-selective mechanism through the order of the pre-synaptic neurons. For example, for a CCW motion, the order of neurons being fired is $1 \to 2 \to 3 \cdots 16 \to 1$. Therefore, the facilitation pulse generated by n_3 can only triggered by the n_4, n_2 produces no trigger pulses.

The STDE and AT-TDE mechanisms take inspirations from asynchronous signal processing methods, which have been widely used in many bio-inspired models [16]–[18], [22]–[26] and neuromorphic systems [27]–[29]. Compared to the well-known differential pair integrator synapse proposed by [29], our STDE and AT-TDE mechanisms only encodes the spike-timing, rather than the spike-rate. Therefore, the AT-TDE is more sensitive to the accelerating motion cues (e.g. the moving object with a larger size, or a sharper contrast generates stronger responses in most models).

The structures of STDE and AT-TDE are displayed in Fig.4. Two neighbouring pre-synaptic neurons (e.g. n_1 and n_2) are connected to the STDE unit by two parallel pre-synapses, of which the pre-synapses are named facilitation and trigger, respectively coloured in red and blue. The AT-TDE is similar to STDE except the two pre-synapses both connects to one single neuron n_{dd}.

The following takes the STDE unit as an example to describe the processing of pulses in detail. The facilitation pulse firstly activates the STDE unit and initializes the gain factor w_e, which decays with the elapse of time. After a short time delay, the trigger pulse is injected into the same STDE unit (see Fig.5(a)).

The amplified I_{trig} and excitatory post synaptic current $EPSC$ could be calculated as:

$$I_{trig} = w_e \cdot I_{fac} + I_{trig}, \tag{3}$$

$$EPSC = I_{trig} \tag{4}$$

After that, the EPSC has been injected into the neuron. As long as the neuron's membrane potential exceeds the threshold, it produces spikes. The neuronal spike unit is described by equation(5):

$$Spike = \begin{cases} 1, & \text{if } e^{EPSC} > u_{thr} \\ 0, & \text{otherwise} \end{cases} \tag{5}$$

where e^{EPSC} is a simplest form to present membrane potential. u_{thr} is a threshold to distinguish the synapses connection strength in temporal scale. Notable that, the u_{thr} is a constant value in STDE but a dynamic value

in AT-TDE unit. Besides, we set an absolute refractory period in the AT-TDE, its duration is 1s.

If the temporal difference between the facilitation pulse and trigger pulse is large, or the trigger pulse arrives before the facilitation pulse, no spike shall be generated (as shown in Fig.5(b) and (c)). In other words, only if facilitation pulse arrives firstly and shortly before trigger pulse, the EPSC amplified strong enough to make the neuronal membrane potential exceed the threshold, and then activates the neuron to produce a spike.

Fig.6 illustrates the functions of STDE and AT-TDE mechanisms in the neuronal pathways. If the translational motion maintains constant velocity, the directional detector generates uniform pulses (see Fig.6(a) and (b) s_{dd} axis). The accelerating detector generates one pulse, only if the $u_{ad}(t)$ firstly exceeds the previous threshold u_{th0}. Subsequently, the threshold has been updated as u_{th1}. The previous threshold u_{th0} and current threshold u_{th1} are stained with red and blue, respectively in Fig.6(c). When the proposed AMPM handing accelerating motions (Fig.6(d)). The temporal difference of successive pluses in direction detector become shorter and shorter. Each pulse with a shorter temporal difference can produce one pulse in the accelerating detector (see Fig.6(e) and (f) s_{dd}, s_{ad}).

III. experiment

This section provide two groups of experiments to test the feasibility and limitations of the proposed model. Since the systematic experimental results of pre-synaptic neural network have been demonstrated in previous work [19], we only present the results of AMPM here.

A. Experimental setup

As show in Fig.7, the experimental videos of translational moving stimuli in panoramic view are synthesized by Matlab. The real-world panoramic static background and dynamic background are captured by the panoramic camera, Insta 360 ONE X. The framerates of all synthetic videos are 60 frames per second. All experiments are implemented on laptop, Windows 11 (CPU: Intel (R) Core (TM) i7-8550U CPU @ 1.80 GHz, RAM: 8GB). Data analysis and visualisations have been conducted in Matlab R2019b. The experimental videos, codes and results can be found at https://github.com/HaoLuan/BIO-INSPIRED-MODEL.

Fig. 7. The synthetic counter-clockwise translational motion in the white background. Red arrow indicates the motion direction. Translating object size: 120 pixels.

B. Demonstrations of the AMPM

In this section, we examined the translational motion directional detector (DD) and accelerating motion detector (AD) with multiple velocities. Firstly, the model is challenged by a group of constant velocities motions within white backgrounds, as shown in Fig.7. In each subgraph of Fig.8, the top axis is the angular velocity of the translational motion. The middle axes donate the CW-DD and CCW-DD spike outputs, respectively stained in blue and red. The bottom axes are the CW-AD and CCW-AD spike outputs. The size of the synthetic translational object is 120 (as same as the experimental video shown in Fig.7). The spikes, which caused by the motions except for the synthetic moving object, are named false positive spikes (as a blue spike in s_{dd} ax, Fig.8(a)). In Fig.8(a), the CCW-DD generates a series of sparse spikes. The temporal difference between two spikes are large enough, thus, the CCW-AD produces no spike. This experimental result is an example of Fig.5(b). The model responses in Fig.8(b)-(c) illustrate that, when the model challenged by the constant velocity motions. The CCW-DD emits uniform spikes, and the CCW-AD only produces one spike at the beginning of the motions. This result is accordingly to Fig.6(b) and (c).

On the other hand, when challenged against accelerating motion, as shown in Fig.8(d)-(e), the CCW-DD produces much more dense spikes. The CCW-AD emits spikes according to the temporal difference change of the two spikes in CCW-DD. In experiment (d), the start velocity of the translational motion is 0.26 rad/s, which is too slow to active the AT-TDE. So, the AT-TDE doesn't generate pulse before 100 frames. When the velocity increases to 0.78 rad/s (after the accelerating at 100^{th} frame), the velocity is big enough to elicit AT-TDE to produce a pluse. When the start velocity is 0.52 rad/s (same as test (b)), the second CCW-DD pulse activates the AT-TDE directly. Notable that, in Fig.8(f), the CCW-AD couldn't generate spikes after 500th frames though the velocity increases. That is because the angular velocity is very large at the moment, the EPSC in TDE unit has been re-activated before it decays enough. Which almost leads to the largest u_{thr} in u_{ad}. The solutions for this could be: (a) improve the sampling rate (i.e. frame-rate of the videos). (b) a higher decay parameter used in TDE unit. (c) multiple neuronal synapses connect to two or more neighbouring neurons of each side (i.e. n_3 connects to n_4 and n_5 and more). As a result, the experiments in this section not only demonstrate the feasibility of the proposed model in detecting accelerating motion, but also show the wide-range adaptation to the velocity changes.

To intuitively illustrate the signal processing in the proposed model, we have made animations to demonstrate the experiments. The animations could be found at https://youtube.com/playlist?list=PLasUMfCjDxFwWaq7ErBQ6Th42ZlqKshV4.

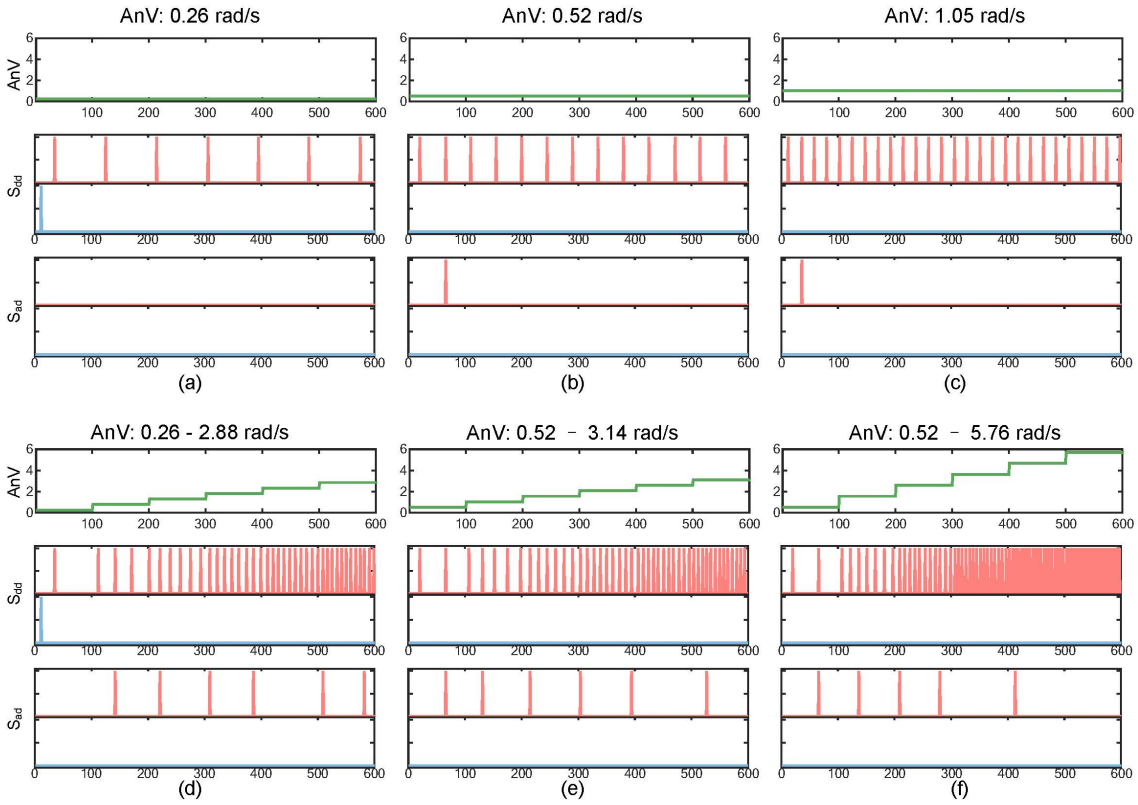

Fig. 8. The model responses to translational motion with constant velocities and accelerating velocities. Green line at the top of each subgraph is the object's angular velocity. In each subgraph, the red spikes represent counter-clockwise motion (CCW) and blue spikes are clockwise motion (CW). AnV: object angular velocity in radian. S_{dd}: directional detector. S_{ad}: accelerating detector. The x-axes denote the number of frames. (a) - (c): Translational motions with three constant velocities, respectively in 0.26 rad/s, 0.52 rad/s and 1.05 rad/s. (d) - (f): Three velocities gradually increased translational motions. (d): Start angular velocity: 0.26 rad/s. Acceleration range: 0.52 rad per 100 frames. (e): Start angular velocity: 0.52 rad/s. Acceleration range: 0.52 rad per 100 frames. (d): Start angular velocity: 0.52 rad/s. Acceleration range: 1.04 rad per 100 frames.

C. Further investigation

To further investigate the limitations of the proposed model, three object sizes and three backgrounds are used to test the model in this section. Fig.9(a) - (c) show three sizes of objects with the same gradually increased velocity. Because the TDE mechanism in the proposed AMPM only encodes spike timing of two successive pulses. It fails to take into consideration the intensity of motions, e.g. the moving object's size and contrast. Consequently, the same velocity motions elicit similar model responses. The differences of model responses are only because the larger object come into the neighbouring receptive field earlier. In addition, the spike frequency adaptation mechanism in the pre-synaptic model also affects the results slightly (see Fig.9(a), Fig.8(a) and (d), a false positive CW-DD spike at the beginning of the motions). The SFA mechanism used in the pre-synaptic model could enhance the neuronal response to approaching stimulus, so it advances the spike timing a little.

Fig.9(d) demonstrates the model response in a static background. Even though the non-uniform luminance of the background causes a false positive spike in CW-DD at the beginning of the motions, the static background doesn't have great impacts on the model responses. It is because the TDE mechanism only encodes spike timing, which reduces the impacts of contrast variances between background and moving object. Fig.9(e) shows the accelerating motion in a chaotic lab, with a man wandering at the corner (green arrows). The object's velocity increases gradually from 0.52 - 3.14 rad/s. The movements of wandering man induce a series dense spikes before 100th frame (see red spikes in DD-spikes in (e)). This series dense spikes enhance the threshold of CCW-AD, thus, only one CCW-AD spike in this experiment. In addition, the movements of wandering man also elicit four false positive spikes in CW-DD (see blue spikes of s_{dd} axis in (e)). This experiment illustrates that the model need a bottom-to-top attention mechanism to continuously focus on wide-field motions instead of local motions. The experiment shown in Fig.9(f) is similar to (e), except the background rotates clockwise additionally. The rotating background movements enhance the object's relative movement velocity. Therefore, the CCW-DD and CCW-AD in this experiment all emit spikes. However, the chaotic and dynamic background also elicit false positive spikes in CW-DD and CW-AD. This experimental result demonstrates

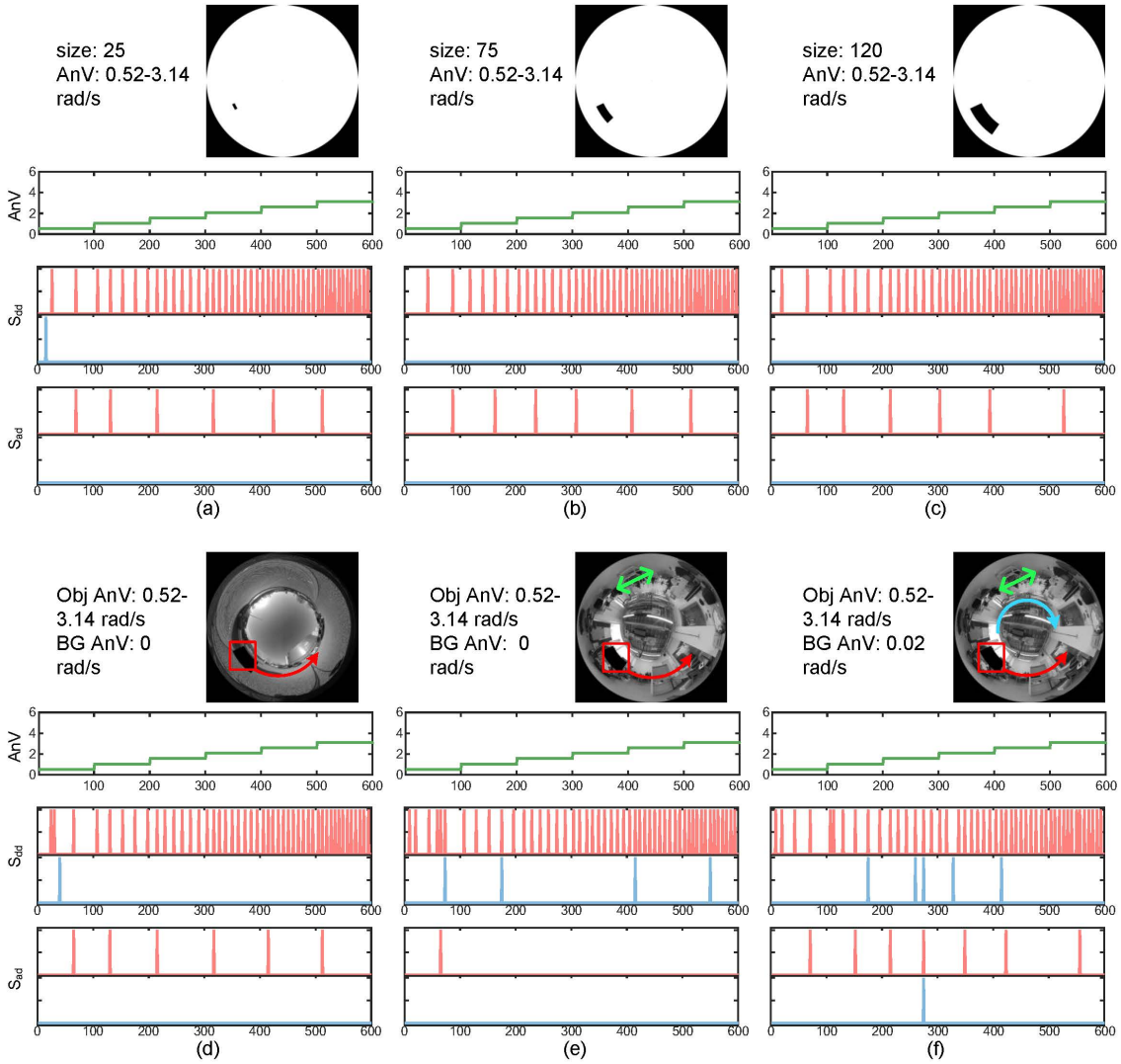

Fig. 9. (a) - (c) Translational motion of objects with the same speed and acceleration but different sizes. (d) An accelerating translational motion (red arrow indicates motion direction) in a static background. (e) The same translational motion happens in a chaotic lab contains a person wandering around the corner (green arrows). (f) The scene is similar to (e), except the whole background rotates clockwise at 0.02 rad/s (blue arrow) in the mean time. In each axis, the red spikes represent counter-clockwise motion and blue spikes are clockwise motion. AnV/Obj AnV : angular velocity in radian. BG AnV: angular velocity of background. S_{dd}: directional detector. S_{ad}: accelerating detector. The x-axes denote the number of frames.

the limitation of the proposed model when challenged by dynamic scene. Whereas, it could be solved by eliminating optical flow information. It should be pointed out that we removed the feed-forward inhibition (FFI) mechanism of the pre-synaptic model here, to prevent it inhibits the neurons from spiking.

IV. Discussion and Conclusion

In the above section, the systematic experiments demonstrate the feasibility and robustness of proposed model in perceiving accelerating motion. The similarity between the model outputs and the LCDCs intracellular recordings in responding to translational motion, also suggests the reasonability of proposed model in simulating the crab's visual neuronal ensemble pathways. Besides, the partial receptive fields of MLG1s are arranged horizontally. Therefore, the AMPM only collects motion cues from horizontal wide field motion, which is also fit the LCDCs' feature of sensitivity to horizontal motion. However, experiments of the proposed AMPM also exhibit the limitations. Although the proposed model can sense accelerating motion in a static background, like the other luminance-changed-based models, dynamic scene is still a huge challenge. In such a complex background, it is unrealistic for one single model to accurately capture motion cues. A better solution is to combine various visual neuronal models to improve the performance. In addition, the lower sampling rate leads to a higher accumulated error, which cannot be ignored when dealing with very fast motions. What's more, such as shown in Fig.8(f), the AMPM could not respond to very fast translational motion. In all experiments, the decaying coefficient of the gain factor has been set to 0.96, so the EPSC could decay below the spiking threshold in around

1s. When challenged by with fast motions, the AT-TDE has been activated too soon, so that its spiking threshold has been updated to the max value. A solution is to set the dynamic decaying coefficient: the decaying coefficient should also be increased after the AT-TDE been activated.

In future research, we will concentrate on following aspects: (a) An optical flow elimination method to inhibit false positive spikes caused by the dynamic background. (b) A model both encodes spike-timing and spike-rate to robustly sense the the moving object. (c) To further investigate the potential of the AMPM in navigation and collision detection of autonomous vehicles and robots.

In summary, we firstly proposed an AMPM to mimic visual neuronal ensemble pathways of crab. The model responses to translational motions prove that our model not only provides a heuristic hypothesis of crab's post-synaptic pathways but, more importantly is demonstrating the excellent robustness in perceiving translational motions with wide range of velocity variations. Furthermore, our systematic experiments illustrate the model's potential when applied in autonomous vehicles due to its reliability and efficiency.

ACKNOWLEDGMENT

This research is supported by the National Natural Science Foundation of China under grant 62020106004, 92048301, and 12031003, the EU's ULTRACEPT project under grant 778062. *Correspondence: qifu@gzhu.edu.cn

References

[1] A. Borst and T. Euler, "Seeing things in motion: models, circuits, and mechanisms," Neuron, vol. 71, no. 6, pp. 974–994, 2011.

[2] F. C. Rind and P. J. Simmons, "Seeing what is coming: building collision-sensitive neurones," Trends in neurosciences, vol. 22, no. 5, pp. 215–220, 1999.

[3] F. Gabbiani, H. G. Krapp, and G. Laurent, "Computation of object approach by a wide-field, motion-sensitive neuron," Journal of Neuroscience, vol. 19, no. 3, pp. 1122–1141, 1999.

[4] D. Tomsic, "Visual motion processing subserving behavior in crabs," Current opinion in neurobiology, vol. 41, pp. 113–121, 2016.

[5] A. Borst, J. Haag, and A. S. Mauss, "How fly neurons compute the direction of visual motion," Journal of Comparative Physiology A, vol. 206, no. 2, pp. 109–124, 2020.

[6] F. C. Rind, S. Wernitznig, P. Pölt, A. Zankel, D. Gütl, J. Sztarker, and G. Leitinger, "Two identified looming detectors in the locust: ubiquitous lateral connections among their inputs contribute to selective responses to looming objects," Scientific reports, vol. 6, p. 35525, 2016.

[7] J. R. Gray, E. Blincow, and R. M. Robertson, "A pair of motion-sensitive neurons in the locust encode approaches of a looming object," Journal of Comparative Physiology A, vol. 196, no. 12, pp. 927–938, 2010.

[8] Q. Fu, S. Yue, C. Hu, J. Peng, C. Rind et al., "A robust collision perception visual neural network with specific selectivity to darker objects," IEEE Transactions on Cybernetics, 2019.

[9] Q. Fu, H. Wang, C. Hu, and S. Yue, "Towards computational models and applications of insect visual systems for motion perception: A review," Artificial Life, vol. 25, no. 3, pp. 263–311, 2019.

[10] K. Nordström, "Neural specializations for small target detection in insects," Current opinion in neurobiology, vol. 22, no. 2, pp. 272–278, 2012.

[11] J. Sztarker and D. Tomsic, "Binocular visual integration in the crustacean nervous system," Journal of Comparative Physiology A, vol. 190, no. 11, pp. 951–962, 2004.

[12] J. Sztarker, N. J. Strausfeld, and D. Tomsic, "Organization of optic lobes that support motion detection in a semiterrestrial crab," Journal of Comparative Neurology, vol. 493, no. 3, pp. 396–411, 2005.

[13] D. Oliva and D. Tomsic, "Visuo-motor transformations involved in the escape response to looming stimuli in the crab neohelice (= chasmagnathus) granulata," Journal of Experimental Biology, vol. 215, no. 19, pp. 3488–3500, 2012.

[14] V. Medan, D. Oliva, and D. Tomsic, "Characterization of lobula giant neurons responsive to visual stimuli that elicit escape behaviors in the crab chasmagnathus," Journal of neurophysiology, vol. 98, no. 4, pp. 2414–2428, 2007.

[15] V. Medan, M. B. De Astrada, F. Scarano, and D. Tomsic, "A network of visual motion-sensitive neurons for computing object position in an arthropod," Journal of Neuroscience, vol. 35, no. 17, pp. 6654–6666, 2015.

[16] S. Yue and F. C. Rind, "Collision detection in complex dynamic scenes using an lgmd-based visual neural network with feature enhancement," IEEE transactions on neural networks, vol. 17, no. 3, pp. 705–716, 2006.

[17] J. Zhao, H. Wang, N. Bellotto, C. Hu, J. Peng, and S. Yue, "Enhancing lgmd's looming selectivity for uav with spatial-temporal distributed presynaptic connections," IEEE Transactions on Neural Networks and Learning Systems, 2021.

[18] Q. Fu, C. Hu, J. Peng, and S. Yue, "Shaping the collision selectivity in a looming sensitive neuron model with parallel on and off pathways and spike frequency adaptation," Neural Networks, vol. 106, pp. 127–143, 2018.

[19] H. LUAN, Q. Fu, Y. Zhang, M. Hua, S. Chen, and S. Yue, "A looming spatial localization neural network inspired by mlg1 neurons in the crab neohelice," Frontiers in Neuroscience, p. 1886, 2022.

[20] D. Oliva and D. Tomsic, "Computation of object approach by a system of visual motion-sensitive neurons in the crab neohelice," Journal of neurophysiology, vol. 112, no. 6, pp. 1477–1490, 2014.

[21] F. Scarano, D. Tomsic, and J. Sztarker, "Direction selective neurons responsive to horizontal motion in a crab reflect an adaptation to prevailing movements in flat environments," Journal of Neuroscience, vol. 40, no. 29, pp. 5561–5571, 2020.

[22] Q. Fu and S. Yue, "Modelling drosophila motion vision pathways for decoding the direction of translating objects against cluttered moving backgrounds," Biological Cybernetics, vol. 114, no. 4, pp. 443–460, 2020.

[23] H. Wang, J. Peng, X. Zheng, and S. Yue, "A robust visual system for small target motion detection against cluttered moving backgrounds," IEEE transactions on neural networks and learning systems, 2019.

[24] H. Meng, S. Yue, A. Hunter, K. Appiah, M. Hobden, N. Priestley, P. Hobden, and C. Pettit, "A modified neural network model for lobula giant movement detector with additional depth movement feature," in 2009 International Joint Conference on Neural Networks. IEEE, 2009, pp. 2078–2083.

[25] Q. Fu, H. Wang, J. Peng, and S. Yue, "Improved collision perception neuronal system model with adaptive inhibition mechanism and evolutionary learning," IEEE Access, vol. 8, pp. 108 896–108 912, 2020.

[26] D. A. Clark, L. Bursztyn, M. A. Horowitz, M. J. Schnitzer, and T. R. Clandinin, "Defining the computational structure of the motion detector in drosophila," Neuron, vol. 70, no. 6, pp. 1165–1177, 2011.

[27] G. D'Angelo, E. Janotte, T. Schoepe, J. O'Keeffe, M. B. Milde, E. Chicca, and C. Bartolozzi, "Event-based eccentric motion detection exploiting time difference encoding," Frontiers in neuroscience, vol. 14, p. 451, 2020.

[28] M. B. Milde, O. J. Bertrand, H. Ramachandran, M. Egelhaaf, and E. Chicca, "Spiking elementary motion detector in neuromorphic systems," Neural computation, vol. 30, no. 9, pp. 2384–2417, 2018.

[29] C. Bartolozzi and G. Indiveri, "Synaptic dynamics in analog vlsi," Neural computation, vol. 19, no. 10, pp. 2581–2603, 2007.